Title:

A high affinity monoclonal antibody against HLA-E-VL9 enhances natural killer cell anti-tumor killing

One Sentence Summary: A high affinity monoclonal antibody against HLA-E-VL9 enhances natural killer cell anti-tumor killing by checkpoint inhibition and antibody dependent cellular cytotoxicity.

Authors: Joyce K. Hwang[1,5,6], Daniel J. Marston[1,5], Daniel Wrapp[1,5], Dapeng Li[1], Marina Tuyishime[2], Simon Brackenridge[3], Brianna Rhodes[5], Max Quastel[3], A. Brenda Kapingidza[5], Jacob Gater[1], Austin Harner[1], Yunfei Wang[1,4], Wes Rountree[1,4], Guido Ferrari[2], Persephone Borrow[3], Andrew J. McMichael[3], Geraldine M. Gillespie[3], Barton F. Haynes[1,6], Mihai L. Azoitei[1,6]

Affiliations: [1]Duke Human Vaccine Institute, Duke University School of Medicine, Durham, NC 27710, USA. [2] Department of Surgery, Duke University School of Medicine, Durham, NC 27710, USA. [3]Nuffield Department of Clinical Medicine, University of Oxford, Oxford OX3 7FZ, UK. 4 Division of Structural Biology, Wellcome Centre for Human Genetics, University of Oxford, Oxford OX3 7BN, UK. [4]Department of Medicine, Duke University School of Medicine, Durham, NC 27710, USA. [5]These authors contributed equally: Joyce K. Hwang, Daniel J. Marston, Daniel Wrapp. Email: joyce.k.hwang@duke.edu, mihai.azoitei@duke.edu, barton.haynes@duke.edu

Abstract:

Natural killer (NK) cells kill target cells following triggering via germline-encoded receptors interacting with target cell-expressed ligands (direct killing), or via antibody-dependent cellular cytotoxicity (ADCC) mediated by FcγRIIIa. NK cytotoxicity is modulated by signaling through activating or inhibitory receptors. A major checkpoint is mediated by the NK inhibitory receptor NKG2A/CD94 and its target cell

ligand, HLA-E, which is complexed with HLA signal sequence-derived peptides termed VL9 (HLA-E-VL9). We have previously reported the isolation of a murine HLA-E-VL9-specific IgM antibody 3H4 and the generation of a higher affinity IgG version (3H4v3). Here we have used phage display library selection to generate a high affinity version of 3H4v3, called 3H4v31, with an ~700 fold increase in binding affinity. We show using an HLA-E-VL9+ K562 tumor model that, in vitro, the addition of 3H4v31 to target cells increased direct killing of targets by CD16-negative NK cell line NK-92 and also mediated ADCC by NK-92 cells transfected with CD16. Moreover, ADCC by primary NK cells was also enhanced in vitro by 3H4v31. 3H4v31 was also able to bind and enhance target cell lysis of endogenously expressed HLA-E-VL9 on human cervical cancer and human pancreatic cancer cell lines. In vivo, 3H4v31 slowed the growth rate of HLA-E-VL9+ K562 tumors implanted into NOD/SCID/IL2rγ^{null} mice compared to isotype control when injected with NK-92 cells intratumorally. Together, these data demonstrate that mAb 3H4v31 can enhance NK cell killing of HLA-E-VL9-expressing tumor cells in vitro by both direct killing activity and by ADCC. Moreover, mAb 3H4v31 can enhance NK cell control of tumor growth in vivo. We thus identify HLA-E-VL9 monoclonal antibodies as a promising novel anti-tumor immunotherapy.

Main Text:

Introduction

Checkpoint inhibition immunotherapy has been a breakthrough in the treatment of cancer and for several malignancies, T cell checkpoint inhibition therapies are now standard of care [1] . Still, most patients do not respond or will relapse after these treatments [2-5] . NK cells are attractive anti-tumor effector cells and have great potential to improve checkpoint inhibition therapies. NK cells can kill tumor cells without prior sensitization [6], bolster adaptive anti-tumor immune responses [7], recognize tumor clones that have evaded T cell immunity by downregulating MHC-Ia [8], and target metastatic tumor cells in circulation [9-11]

NK cells interrogate potential targets with germline encoded activating or inhibitory receptors. Target cell killing by NK cells is triggered when net signaling through activating receptors is stronger than through inhibitory receptors. NK cytotoxicity may proceed solely through direct interaction of NK cell germline-encoded receptors with ligands for activating NK receptors that have been upregulated and/or ligands for inhibitory NK receptors that have been downregulated on the targets [12], or by sensitization of targets by antibody Fab binding with triggering of NK killing through Fcγ receptor (FcγR)-engagement [13].

The inhibitory NKG2A/CD94 heterodimeric receptor, expressed on ~40% of peripheral blood NK cells and 5% of CD8+ T cells in healthy individuals [14, 15] is a key potential immune checkpoint. The NK inhibitory molecule, NKG2A/CD94 binds to the minimally polymorphic HLA class Ib molecule HLA-E on target cells [16-19]. Surface expression of HLA-E is stabilized by a restricted subset of peptides VMAPRT (L/V)(V/L/I/F)L (designated VL9) derived from the leader sequence of HLA-Ia molecules, facilitating engagement of HLA-E with NKG2A/CD94 [16-19]. HLA-E is constitutively expressed at low levels on most normal tissues but highly expressed in certain tissues such as placenta [20] where HLA-E-VL9 placental cell interactions with NK NKG2A/CD94 are hypothesized to mediate tolerance to the fetus [21]. HLA-E is also capable of binding to host stress associated peptides derived from heat shock protein 60 (Hsp60) [22], peptides from multidrug resistance associated protein 7 [23], peptides from mycobacterium tuberculosis [24, 25], peptides from retrovirus Gag proteins [26] and EBV-associated peptides [27, 28].

HLA-E is overexpressed in a diversity of tumors, including cervical and ovarian cancers [29], colorectal cancers [30] [31] [32], lung cancers [33], and chronic lymphocytic leukemia [34], and has been shown to be further upregulated by signals within the tumor microenvironment suggesting delivery of NK inhibitory signals by the tumor or tumor microenvironment [11, 35-38]. Overexpression of HLA-E and high levels of NKG2A on NK cells each has been correlated with poor disease outcomes [33, 38-41].

Current therapies directed against the HLA-E/NKG2A axis have had promising but limited success. The anti-NKG2A monoclonal antibody monalizumab effectively enhanced NK and T cell killing of tumors, and was well-tolerated in an early phase trial with cetuximab in previously treated squamous cell carcinoma of the head and neck [42], however, the phase III INTERLINK-1 trial did not demonstrate survival benefit [43]. An anti-HLA-E-VL9 mAb is an alternative method of HLA-E/NKG2A checkpoint inhibition that could not only enhance NK cytotoxicity of tumor cells, but could also simultaneously mediate tumor cell ADCC [44, 45].

Our group previously reported the discovery of an HLA-E-VL9 (3H4) antibody that when affinity matured enhanced NK killing in vitro [46]. Here, we have further affinity matured this antibody (3H4v31) and demonstrated its ability to enhance NK cell anti-tumor killing in vitro by NK and ADCC effector functions and to enhance NK cell line-mediated retardation of tumor growth in vivo. Finally, 3H4v31 recognized HLA-E-VL9 on certain malignant cell lines and mediated their killing by NKG2A+ NK cells. We thus identify HLA-E-VL9 monoclonal antibodies as a promising novel anti-tumor immunotherapy.

Results:

Generation of a high-affinity monoclonal antibody against anti-HLA-E-VL9

To optimize mAb 3H4v3 IgG binding to cell surface HLA-E-VL9 [46], we further used additional rounds of *in vitro* affinity maturation using yeast surface display to select for mutations that increased HLA-E-VL9 affinity (**Figure 1A**). Based on structural analysis [46], three sites located in the CDRH3 loop of 3H4v3 mAb were simultaneously randomized to sample all 20 possible amino acids. After four rounds of selection with decreasing HLA-E-VL9 concentration, the library was dominated by one clone, named 3H4v31, that contained three additional mutations relative to the 3H4v3 template (S^{100a}→R, Y^{100b}→W, G^{100c}→N). The recombinantly expressed 3H4v31 IgG1 antibody bound to HLA-E VL9 with an affinity of 11.5 nM, representing a 19-fold increase over the previously engineered 3H4v3 and a ~4300-fold increase compared to the original wildtype (WT) 3H4 [46] (**Figure 1B**).

The crystal structure of 3H4v31 Fab confirmed that the affinity maturation process altered the CDRH3 loop without affecting the global conformation of the 3H4 Fab (**Figure 1C**). Structural alignment between 3H4v3 and 3H4v31 mAbs resulted in an RMSD of 1.464 Å over 401 Cα atoms, with the major structural differences located in the CDRH3 loop and with minor differences due to the orientation between the Fab variable and constant domains. Alignment of the newly determined structure of 3H4v31 to the previously determined co-crystal structure of 3H4 WT bound to HLA-E-VL9 (Li et al., Comm Bio 2022) (PDB ID: 7BH8) revealed the optimized interaction network between the HLA-E-VL9 complex and the affinity-matured CDRH3 (**Figure 1D**). In particular, the engineered tryptophan at position 100b (Kabat numbering) is predicted to interact with both Arg62 from the HLA-E heavy chain and Pro4 from the VL9 peptide. The new 3H4v31 CDRH3 loop is predicted to increase the amount of buried surface area over the VL9 peptide and the HLA-E peptide-binding cleft, perhaps contributing to the enhanced peptide specificity of 3H4v31 relative to WT 3H4 that cross-reacts with certain pathogen-derived HLA-E peptide complexes (**Figure 1E).**

FIGURE 1

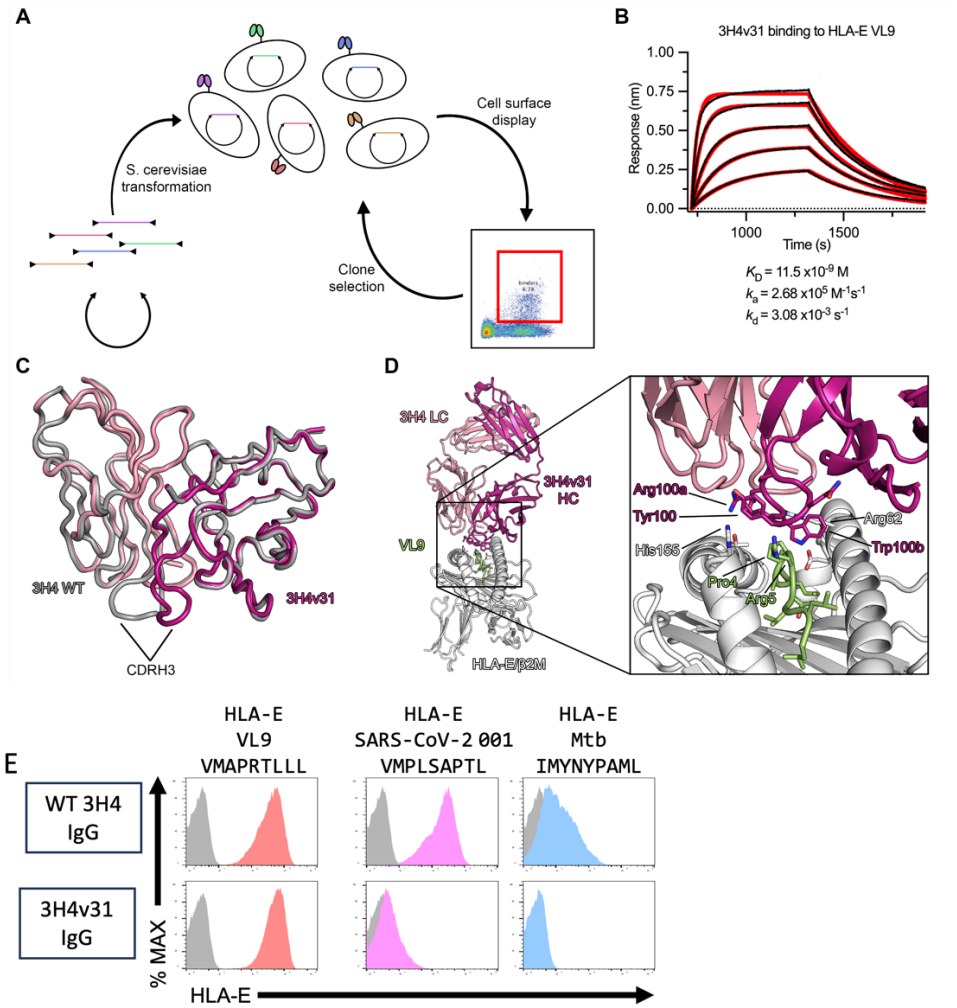

Figure 1: Development and characterization of 3H4v31, an affinity-matured HLA-E-VL9-directed monoclonal antibody. (**A**) Diagram depicts the in vitro affinity maturation process. Mutant scFv plasmid libraries are transfected into yeast and scFv's are displayed on the cell surface. Clones that enhance HLA-E-VL9 binding are then iteratively enriched through fluorescence activated cell sorting. (**B**) Binding of 3H4v31 to HLA-E-VL9 was measured by biolayer interferometry (BLI). Binding data are shown as black lines and the best fit of a 1:1 binding model is shown as red lines. (**C**) The crystal structure of 3H4v31 is shown as ribbons, with the heavy chain colored dark pink and the light chain colored light pink. The previously determined crystal structure of 3H4 WT (PDB ID: 7BH8) has been aligned based on the position of the heavy chain and is colored gray. (**D**) The crystal structure of 3H4v31 is shown, aligned to the previously determined complex of 3H4 WT bound to HLA-E VL9. 3H4v31 is colored according to panel C, the HLA-E heavy chain and B2M are colored white and the VL9 peptide is colored green. Inset shows a zoomed-in view of the predicted 3H4v31 binding interface. Predicted contact residues and residues that vary between 3H4 WT and 3H4v31 are shown as sticks. Oxygen atoms are colored red and nitrogen atoms are colored blue. **(E)** The specificity of binding of 3H4v31 to HLA-E-VL9 was assessed by transfecting 293T cells with a panel of plasmids encoding as single chain trimers of HLA-E, beta-2-microglobulin, and peptide: HLA-E-VL9, HLA-E-VMPLSAPTL derived from SARS-CoV-2, and HLA-E-IMNYPAML derived from M. tuberculosis. Transfectants were stained with WT 3H4 and 3H4v31 IgG, followed by an anti-human IgG secondary antibody.

3H4v31 enhances NK mediated natural cytotoxicity and ADCC in vitro

To determine if binding of 3H4v31 to HLA-E-VL9 on target cells could enhance NK killing in vitro, we used chromium release assays [46, 47] to measure NK killing of a K562 human leukemia cell line modified to express HLA-E-VL9 (K562-HLA-E-VL9) as a single chain trimer of HLA-E, beta-2-microglobulin, and peptide [48]. First, we assayed direct cytotoxicity by testing killing by NK-92, a NKG2A/CD94-positive human NK cell line that lacks CD16/ FcγRIIIa; cytotoxicity observed with NK-92 is therefore direct killing and ADCC-independent. Cytotoxicity was decreased against K562-HLA-E-VL9 targets compared to K562, demonstrating the suppressive capacity of HLA-E-VL9 on killing by NK-92 **(Figure 2A).** Cytotoxicity was reduced at effector: target (E:T) ratios of 1:1 (3-fold reduction) and 5:1 (2-fold reduction), and we therefore used an intermediate E:T ratio of 2.5:1 for subsequent experiments. The addition of 3H4v31 IgG1 enhanced NK-92 killing of K562-HLA-E-VL9 by 1.5 to 2.2-fold, over a range of tested concentrations between 0.016 μg/mL to 10 μg/mL, with a dose dependent relationship (Kendall Tau correlation = 0.5450, P = 0.0004) (**Figure 2B).** We confirmed that 3H4v31 IgG1 had no intrinsic cytotoxic capacity when added to K562-HLA-E-VL9 cells in the absence of NK cells (**Figure 2C)**; rather, enhancement of cytotoxicity depended on the presence of NK cells in the co-culture. Comparing NK killing between that achieved with high HLA-E-VL9 affinity 3H4v31 IgG1 versus with low affinity WT 3H4 IgG1 demonstrated greater NK killing with 3H4v31 versus WT 3H4 (**Figure 2B**), demonstrating that enhancement of NK killing was a function of Fab affinity for HLA-E-VL9**.** At each tested concentration, 3H4v31 IgG1 mediated at least equal levels of NK killing compared to anti-NKG2A IgG. Thus, high-affinity anti-HLA-E-VL9 mAb 3H4v31 IgG1 enhanced NK cell mediated natural cytotoxicity of K562-HLA-E-VL9 targets.

FIGURE 2

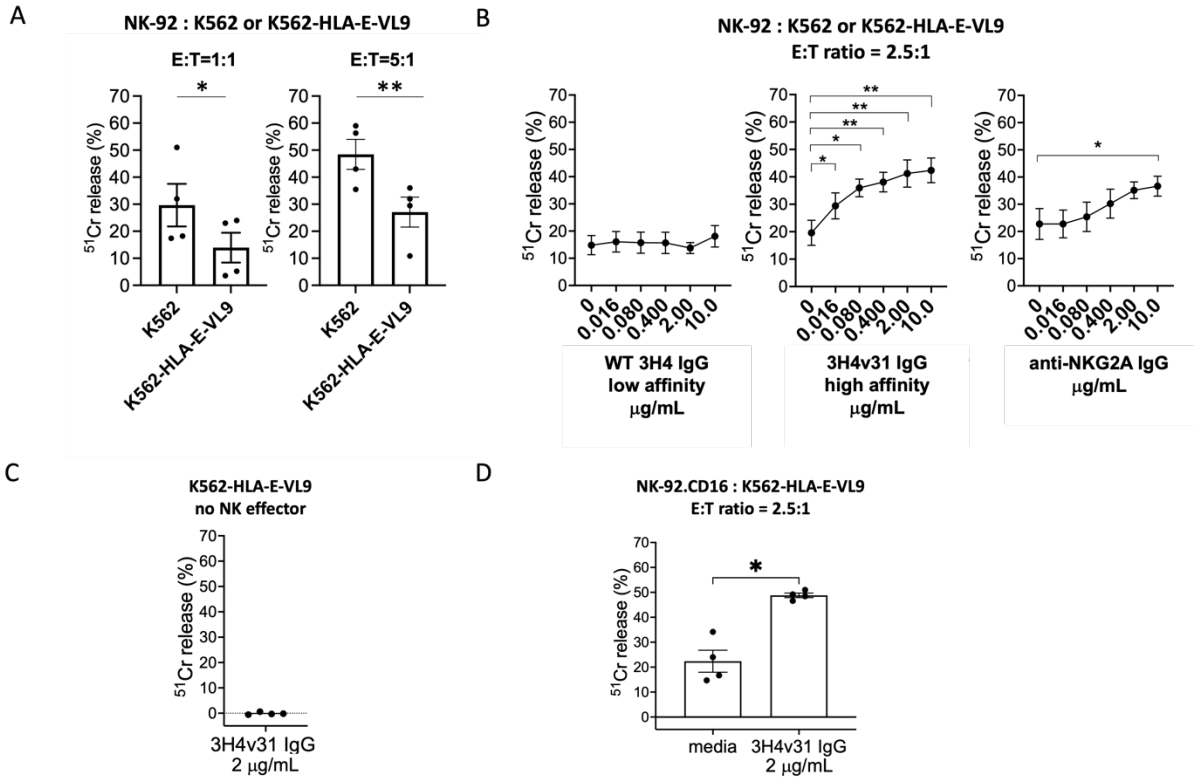

Figure 2: anti-HLA-E-VL9 mAb enhances target cell killing by NK cells. NKG2A+ NK cell line NK-92 cells were co-cultured with K562-HLA-E-VL9 target cells, at the indicated effector:target (E:T) ratios. Target cell lysis was quantified by ^{51}Cr release after 6 hours of effector and target co-culture. (**A**) Target cell killing of K562 or K562-HLA-E-VL9 target cells by NK-92. Dots represent means of independent experiments. (**B**) Target cell killing by NK-92 NK cells in the presence of increasing concentration of monoclonal antibodies: wildtype 3H4 IgG1 with low affinity of HLA-E-VL9 (left), affinity-matured 3H4 v31 IgG1 (middle), or anti-NKG2A (right). Dots and error bars represent mean and SEM of three-four replicates. **(C)** 3H4v31 mAb at 2 μg/mL was added to a culture of K562-HLA-E-VL9 target cells. Target cell lysis was quantified by ^{51}Cr release after 6 hours of effector and target co-culture. Dots represent means of independent experiments. **(D)** Target cell killing by NK-92.CD16 with media versus 2 μg /mL of 3H4v31. Dots represent means of independent experiments. Statistical analysis was performed by two-sided paired t-tests. Asterisks indicate statistical significance between groups: * $P<0.05$, ** $P<0.01$.

We next asked whether in addition to enhancing natural cytotoxicity, 3H4v31 might also enhance NK mediation of ADCC. For these experiments we used an ADCC-capable variant of NK-92 transduced with CD16 (NK-92.CD16) [49, 50]. Like NK-92, NK-92.CD16 cells had enhanced cytotoxicity with 3H4v31 (**Figure 2D**), representing the combined effects of both increasing direct killing by blocking HLA-E interaction with NKG2A and mediating ADCC. We tested for ADCC by using flow cytometry to measure NK degranulation based on CD107a+ surface expression of effectors upon co-culture with targets in the presence of test antibodies. We tested antibodies at 1 μg/mL, which represented an intermediate concentration of 3H4v31 that had enhanced direct cytotoxicity (**Figure 2B**). We observed that NK-92.CD16 cells exhibited substantial degranulation upon coculture with K562-HLA-E-VL9 in the presence of 3H4v31 **(Figure 3A)**, well above the level mediated by a version of 3H4v31 with mutations in L234A, L235A and P329G that abrogates Fc-FcR mediated functions (3H4v31_LALA) [51]. Non-affinity matured WT 3H4 mAb, isotype control antibody CH65 that does not bind HLA-E-VL9, and anti-NKG2A IgG elicited background levels of degranulation **(Figure 3A).** Thus, 3H4v31 enhanced Fc degranulation-mediated killing by NK-92.CD16 cells. Though 3H4v31 had enhanced target cell killing by NK-92 effectors as measured by ^{51}Cr (**Figure 2B**), degranulation of NK-92 cells was not substantially increased with 3H4v31, likely reflecting the high sensitivity of the ^{51}Cr assay for target cell death and lower sensitivity of the degranulation assay for sufficient effector activation to generate detectable accumulation of CD107a on the cell surface mediated by CD107a-independent pathways (**Figure S1**). To determine if PBMC NK cell mediation of ADCC could also be enhanced, we repeated the study in Figure 3A but with primary NK cells instead of NK-92 cells. We found 3H4v31 enhanced ADCC in primary NK cells isolated from the peripheral blood of three donors (**Figure 3B**). In sum, 3H4v31 IgG1 enhanced ADCC by NK-92.CD16 cells and primary CD16+ NK cells.

FIGURE 3

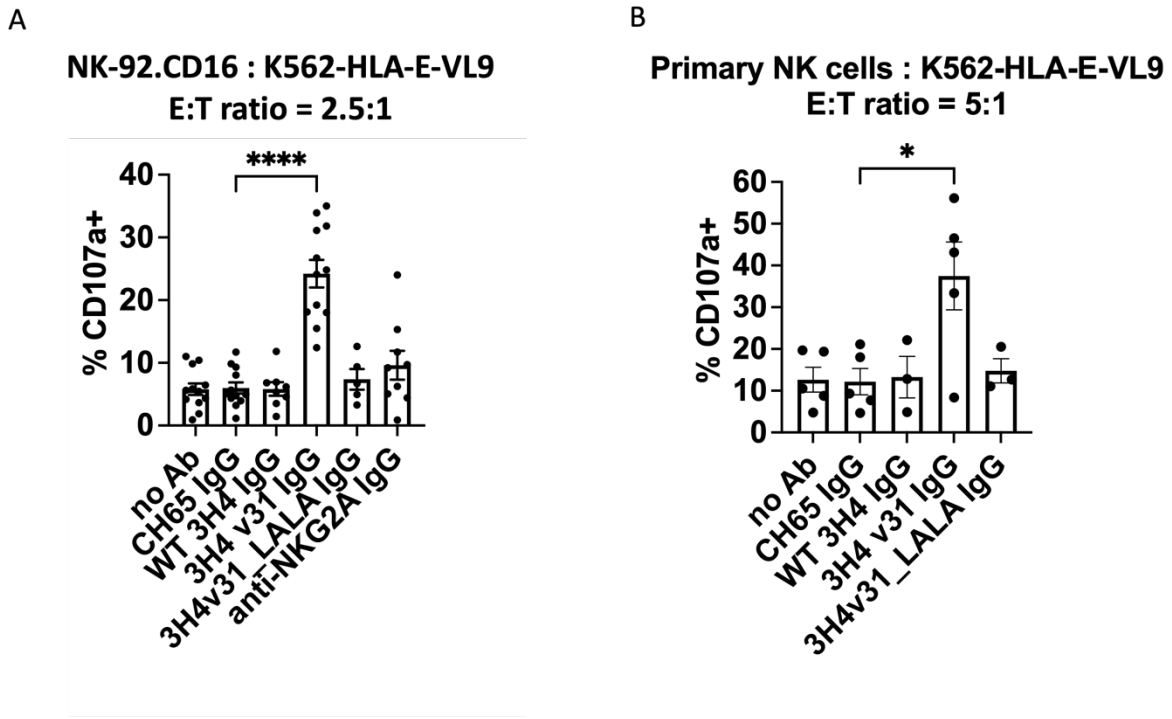

Figure 3: anti-HLA-E-VL9 mAb enhances degranulation and ADCC by NK cells. NK effectors were co-cultured with K562-HLA-E-VL9 target cells as the indicated effector:target (E:T) ratios. ADCC is assessed by degranulation of NK cells as measured by CD107a positivity with the addition of test antibodies to the co-culture. **(A)** Degranulation of NK-92 transfected with CD16 (NK-92.CD16) with addition of mAbs 3H4v31 IgG, no antibody (no Ab), isotype control (CH65), low affinity wildtype 3H4 (WT 3H4), 3H4v31 IgG with LALA Fc mutation (3H4v31_LALA), and anti-NKG2A. **(B)** Degranulation of human primary NK cells isolated from 5 individuals with addition of mAbs 3H4v31 IgG, no antibody (no Ab), isotype control (CH65), low affinity wildtype 3H4 (WT 3H4), 3H4v31 IgG with LALA Fc mutation (3H4v31_LALA), and anti-NKG2A. Statistical analysis was performed by two-sided paired t-tests. Asterisks indicate statistical significance between 3H4v31 and isotype control: * $P<0.05$, ** $P<0.01$, *** $P<0.001$

3H4v31 enhanced tumor control *in vivo*

We next asked if the 3H4v31 enhancement of NK killing of K562-HLA-E-VL9+ AML cells *in vitro* could translate into an anti-tumor effect *in vivo.* We used immunodeficient NOD/SCID/IL2rγ^{null} (NSG) mice, which have complement and most innate immune components including macrophages and monocytes but lack endogenous B, T, or NK cells, permitting assessment of activity of adoptively transferred NK cells. We implanted K562-HLA-E-VL9 tumors subcutaneously into the right flank of NSG mice, which manifested palpable tumors 1-2 weeks after implantation. Mice were treated on days 10, 14, 16, and 18 post tumor implantation with intra-tumoral injection of NK-92 cells and IL-2 in addition to either 3H4v31 IgG1 (NK-92 cells with 3H4v31 treatment group) or isotype control IgG1 (NK-92 cells with isotype control antibody group) (**Figure 4A**). IL-2 was provided with these treatments to enhance NK-92 viability. An additional group received CH65 and IL-2 without NK cells (isotype control antibody without NK cells group). As expected, the tumor growth rate of the NK-92 cells with isotype control antibody group was similar to that of the isotype control antibody without NK cells group, consistent with NK cell inhibition by the K562-HLA-E-VL9 tumor. In contrast, tumor growth rate was significantly slowed in the NK-92 cells with 3H4v31 treatment group: 769 mm3 per day from days 10 to 18 in the 3H4v31 treatment group, compared to 2902 mm3 per day for the NK-92 cells with isotype control antibody group (mixed effect model, p=0.00006) and compared to 2733 mm3 per day for the isotype control antibody without NK cells group (mixed effect model, p = 0.0000008).

Despite being immune deficient, NSG mice still contain some immune cells that may mediate antibody dependent effects, such as macrophages and monocytes whose effector functions can be promoted by antibody dependent cellular cytotoxicity and phagocytosis [52]. To test if 3H4v31 may be able to exert a protective effect by NK-independent as well as NK-dependent mechanisms, we included in our next iteration of the experiment a group treated with 3H4v31 and IL-2, without NK cells. K562-HLA-E-VL9 tumors were implanted subcutaneously into NSG mice and treated on days 11, 13, 15, 17, and 19 with intratumoral injection of 3H4v31, NK-92, and IL-2 (NK-92 cells with 3H4v31 treatment group) ; CH65, NK-92, and IL-2 (NK-92 cells with isotype control antibody group); or 3H4v31 and IL-2 (3H4v31

without NK cells group) (**Figure 4B**). Tumors were on average larger at the time of first treatment (645 mm3 rather than 170 mm3 in the first experiment), nevertheless, growth rate was again slower in the NK-92 cells with 3H4v31 treatment group compared to in the NK-92 cells with isotype control group. The tumor growth rate in the 3H4v31 without NK cells group was intermediate between the two. Though not statistically significantly different from that of either the NK-92 cells with 3H4v31 treatment group or NK-92 cells with isotype control antibody group, the intermediate growth rate of the 3H4v31 without NK-92 cells group could not rule out a weaker 3H4v31-mediated tumor control effect (**Figure 4B**). Slowing of tumor growth with treatment with NK-92 cells with 3H4v31 compared to treatment with NK-92 cells with isotype control as well as the intermediate phenotype of 3H4v31 treatments delivered without NK cells, were reproduced in an additional experimental replicate **(Figure 4C).**

FIGURE 4

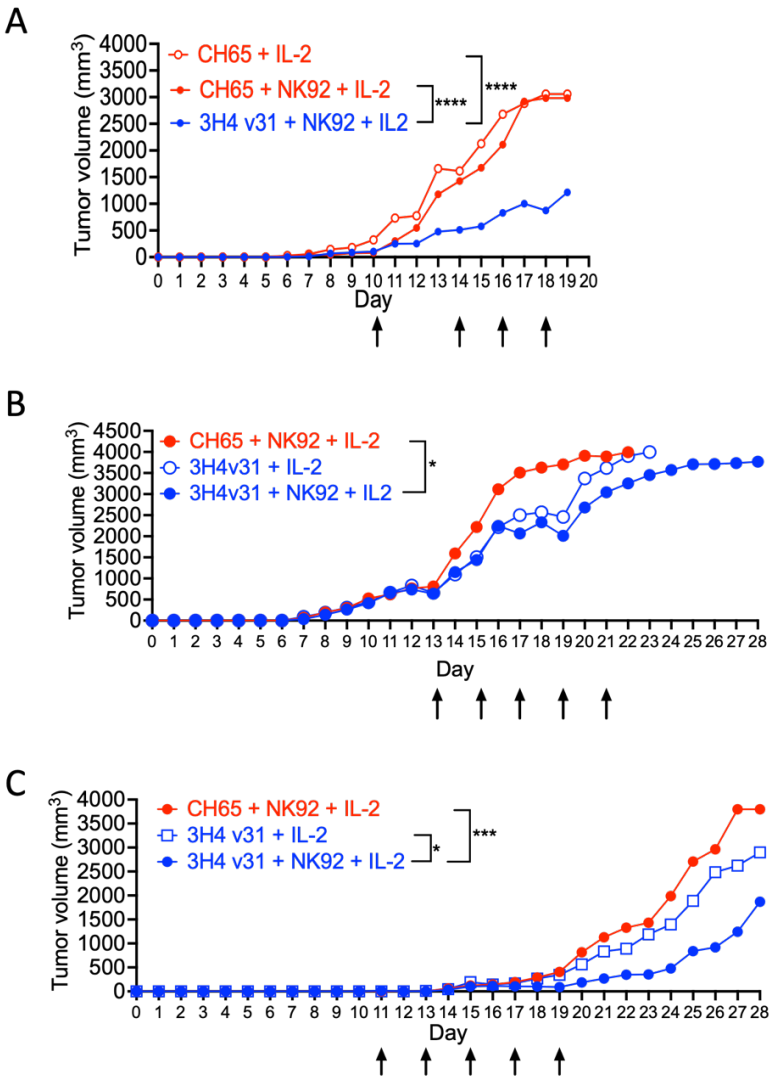

Figure 4: 3H4 v31 treatment retards HLA-E-VL9 expressing tumor growth *in vivo.* NSG mice were implanted subcutaneously with K562-HLA-E-VL9 cells. On the days indicated (arrows), mice received treatments comprised of intratumoral injection of mixtures of effectors and/or mAbs and/or IL-2. Tumors were measured daily, and mice were euthanized at a prespecified endpoint per study of 2000 mm3 (for experiment shown in (A) or 3375 mm3 for (B-C). **(A)** Mice were treated with 900 micrograms of 3H4 v31 anti-HLA-E mAb, 10 million NK-92 cells, and 25000 IU of IL-2 (blue closed circles); 900 micrograms of CH65 anti-flu antibody as isotype control, 10 million NK-92 cells, and 25000 IU of IL-2 (red closed circles); or 900 micrograms of CH65 and 25000 IU IL-2 (red open circles). N=5 mice per treatment group. **(B)** Mice were treated with 3H4 v31 + NK-92 + IL-2 (blue closed circles), CH65 + NK-92 + IL-2 (red closed circles), and 3H4 v31 + IL-2 (blue open circles). N=10 mice. **(C)** Mice were treated with 3H4 v31 + NK-92 + IL-2 (blue closed circles), CH65 + NK-92 + IL-2 (red closed circles), and 3H4 v31 + IL-2 (blue open circles). N=11 mice. Statistical analysis was performed using mixed effects models of tumor growth rate. Asterisks indicate statistical significance. * P<0.05, *** P<0.001, **** P<0.0001

To visualize the cellular interactions underlying the anti-tumor effect of 3H4v31 in the presence of NK cells, we treated tumors with one dose of NK-92 cells with 3H4v31 or NK-92 cells with CH65 isotype control antibody and harvested tumors 28 hours afterwards for immunohistochemistry (IHC). Sections were formaldehyde-fixed and stained with anti-CD56 antibodies to detect NK cells and anti-cleaved caspase 3 to detect activated caspase as a marker of apoptotic cell death. Tumor sections from mice treated with NK-92 cells and isotype control CH65 demonstrated the presence of NK-92 cells. Apoptosis was detected at higher levels in the 3H4v31 treated tumors compared to the CH65-treated tumors consistent with enhancement of NK mediated cytotoxicity (**Figure 5A**). In addition, we verified the presence of endogenous CD16/32 bearing cells that could account for the weak NK-independent effect of the 3H4v31 antibody we had observed in our in vivo studies by staining the tumor sections with anti-mouse CD16/32 **(Figure S2)**. Endogenous CD16 bearing innate immune cells made contacts with apoptotic cells and 3H4v31 (**Figure S3**).

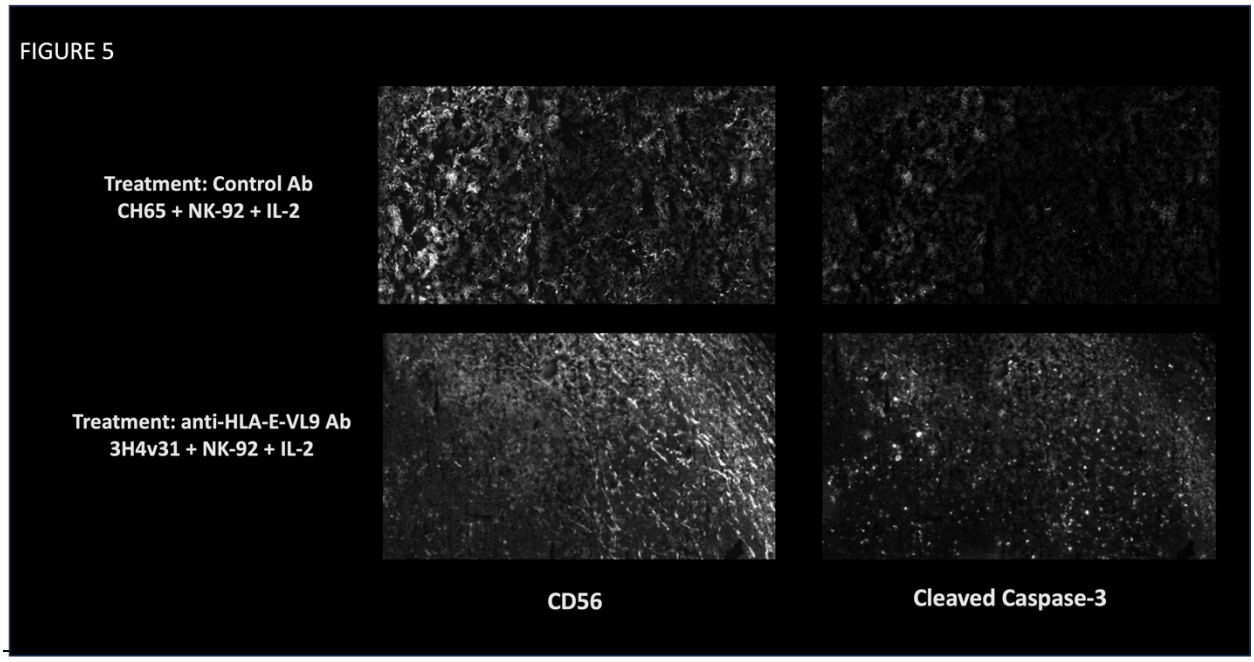

Figure 5: 3H4v31 and NK cell treatment increases apoptotic cell death *in vivo.* Tumors treated with one dose of 3H4v31 + NK-92 cells + IL-2 treatment (lower panels) or isotype control mAb CH65 and NK-92 cells and IL-2 (upper panels) were harvested and cryopreserved 28 hours later. Sections were fixed and stained with anti-CD56 antibodies to detect NK-92 cells (left) and anti-cleaved caspase-3 antibodies to detect activated caspase as a marker of apoptosis (right).

3H4v31 binds to select human cancer cell lines

We next evaluated whether the strong anti-tumor effect we observed with 3H4v31 on targets expressing HLA-E-VL9 as a single chain trimer could be extended to HLA-E-VL9 that is endogenously processed and expressed on tumor cells. We identified two human cancer cell lines with endogenous expression of HLA-E-VL9 based on flow cytometry assessment of binding of the cell lines to 3H4v31 **(Figure 6A):** SiHa (a cervical cancer cell line) and SU86.86 (pancreatic ductal adenocarcinoma cell line). In chromium release assays killing of these cell line targets by NK-92.CD16 were also enhanced **(Figure 6B**). Thus, 3H4v31 binds and mediates enhanced NK killing of human cancer cell lines with endogenously assembled and expressed HLA-E-VL9.

FIGURE 6

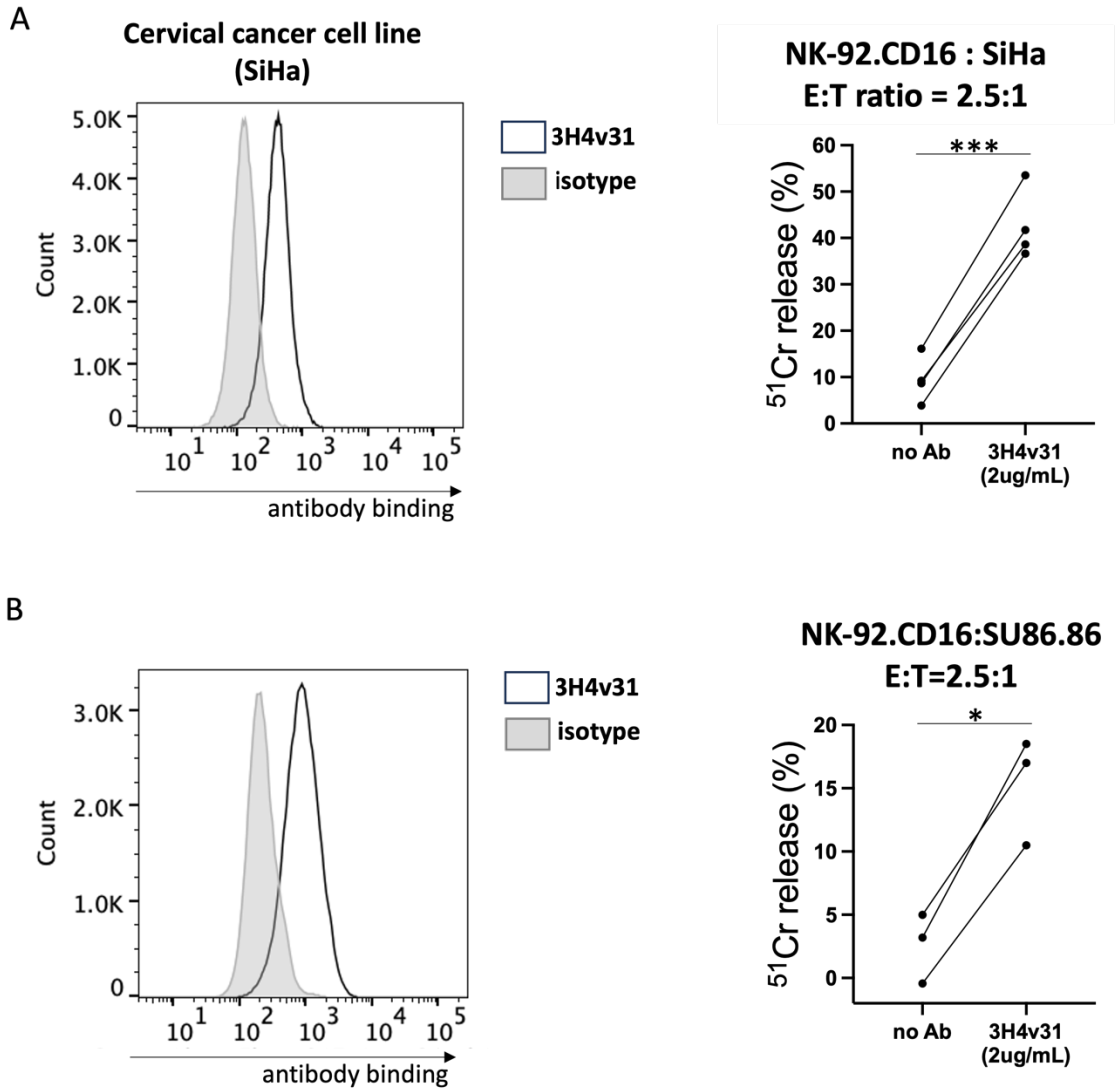

Figure 6: HLA-E-VL9 cell surface expression and 3H4v31 binding on cancer cell lines.
Flow cytometry analysis of 3H4v31 binding to SiHa (A), and SU86.86 (B). Left: Cells were stained with 4 μg/mL 3H4v31, then with an anti-human IgG AF647 secondary antibody (black unshaded peaks). An isotype control stain is shown for comparison (grey shaded peaks). Right: NK-92.CD16 cells were co-cultured with cell lines at E:T ratio of 2.5:1. Target cell lysis was quantified by ^{51}Cr release after 6 hours of effector and target co-culture Dots represent means of independent experiments. * $P<0.05$, *** $P<0.001$

Discussion:

We previously described the discovery of HLA-E-VL9 binding B cells from the naive repertoire of mice and humans, and showed that with sufficient affinity anti-HLA-E mAbs can interrupt the interaction of HLA-E-VL9 and NKG2A/CD94 and thereby enhance NK cytotoxic killing [46]. Here we report the generation of a high affinity mAb specific to HLA-E-VL9, 3H4v31, and demonstrate its ability to enhance anti-tumor killing by NKG2A+ NK cell lines in vitro and in vivo, enhance direct killing and ADCC activity, and activate primary NK cells against HLA-E-VL9 expressing tumor targets.

Current therapeutics targeting the NKG2A:HLA-E axis comprise the anti-NKG2A mAb monalizumab, which has had promising but limited success (INTERLINK-1 trial). Our work sought to improve on the status quo by exploring the anti-tumor efficacy of targeting the other end of the NKG2A:HLA-E axis. As above, we found that targeting HLA-E engages ADCC as well as enhances direct killing. Additionally, IgG Fc's are known to also mediate ADCP by neutrophils/macrophages. Though not explicitly tested in our system, we think it is likely that ADCP accounts for the intermediate growth rate of tumors treated with 3H4v31 without NK effectors (faster than that of tumors treated with 3H4v31 and NK-92 cells and slower than that of CH65 with NK-92 cells) in our in vivo experiments; endogenous neutrophils and monocytes are present in NSG mice [53] and IgG Fc is known to mediate significant ADCP . Specific mutations of the Fc domain could permit the tuning of 3H4v31 mediated enhancement of ADCC, ADCP, or both depending on the desired immune cells engaged [54]. Thus, anti-HLA-E mAb therapy has the potential to increase innate immune cell killing by multiple pathways, and thereby contributes to efforts to improve on the anti-tumor effect of a NKG2A:HLA-E targeting approach.

From a translational perspective, we envision that an anti-HLA-E-VL9 mAb like 3H4v31 could be administered on its own to activate endogenous primary NK cells as demonstrated in our *in vitro* studies, or in combination with adoptively transferred NK cells. The NK-92 cell line that we tested in our *in vivo* studies already has FDA IND approval for use in human clinical trials. Early phase trials of NK-92 cell infusions have shown good tolerability and achieved clinical responses in some cases of melanoma,

lung cancer, AML, Hodgkin Lymphoma, and multiple myeloma, among others [55, 56]. We anticipate that 3H4v31 should also increase the activity of NK adoptive cell therapies in development such as CAR NK's, which are of growing interest for their safety relative to CAR T cells and potential for use as off-the-shelf therapy [57]. Additionally, an anti-HLA-E-VL9 mAb may also enhance the anti-tumoral activity of the subset of CD8+ T cells with NKG2A [14, 15].

The main limitations of this work are three-fold. We do not address the effect that HLA-E blockade may have on the additional interaction that HLA-E has with NKG2C/CD94, an activating NK receptor. The binding affinity of HLA-E-VL9 for NKG2A/CD94 is greater than that for NKG2C/CD94 such that the inhibitory signal likely dominates when both NKG2A+ and NKG2C+ cells are present [17, 19, 58], but how this may affect control of a disease state in which NKG2C+ NK cell activity is unknown; we would expect that at least CD16+ NKG2C+ NK cells (i.e. with CD16) should have enhanced activity against HLA-E expressing targets via ADCC, but this remains to be tested. Secondly, our *in vivo* model of intratumoral injection does not represent routes of adoptive cell or other infusional therapies as they are typically delivered in the clinic (i.e. intravenously), and so translating anti-HLA-E-VL9 mAb to the clinic will involve demonstrating its activity when delivered systemically. Thirdly, while HLA-E-VL9 is over-expressed on tumors relative to normal tissues, and further increased by signals within the tumor microenvironment [11, 35-38] , off-target effects are still an important concern that will be key to address to translate anti-HLA-E mAb therapy to the clinic. Promisingly, our anti-HLA-E-VL9 mAb had no intrinsic cytotoxicity (**Figure 2C**), thus, its anti-tumor activity is still subject to the immunological checks and balances related to cytotoxic effector recruitment to tissues and integration with other activating/inhibitory signals on effector functions. In addition, two existing therapies that modulate the NKG2A:HLA-E axis, the anti-NKG2A mAb monalizumab, and the nuclear export protein exportin-1 inhibitor selinexor that acts partly through HLA-E downregulation [37, 59], have both been well tolerated in people. Nevertheless , should off-target effects prove prohibitive, future studies of anti-HLA-E therapy may alternatively focus on stress- and tumor-specific HLA-E peptides [23, 28, 60]. In this regard, we confirmed here that affinity maturation of 3H4 can be achieved that yields changes localized to the CDR

loops and without destabilizing the global conformation of the Fab (**Figure 1**), thus we anticipate that mAbs specific to complexes of HLA-E with tumor specific peptides should be able to be generated by in vitro affinity maturation or other approaches.

In summary, we demonstrated that an HLA-E-VL9 specific mAb can enhance anti-tumor killing in vitro and in vivo, by NK cell lines and human primary NK cells, against HLA-E-VL9 expressing targets, via ADCC as well as direct killing. We thus provide proof of principle for anti-tumor activity of anti-HLA-E based monoclonal antibody therapy, which given the overexpression of HLA-E on multiple tumor types could have broad applicability.

Materials and Methods:

Protein production for crystallographic studies

The HLA-E-VL9 complex was purified from bacterial inclusion bodies as described previously [46]. Briefly, Rosetta 2(DE3) cells (Novagen) were transformed with plasmids encoding for the HLA-E*0103 heavy chain and beta-2 microglobulin. Cells were induced with 1 mM IPTG at an OD600 of 1.00 and harvested after 18 hours of expression at 20° C. Cells were lysed by sonication in buffer composed of PBS with cOmplete EDTA-free protease inhibitor (Roche) and universal nuclease (Pierce). Lysates were cleared by ultracentrifugation and pelleted inclusion bodies were washed twice with detergent buffer (0.5% Triton X-100, 50 mM TRIS pH 8.0, 100 mM NaCl, 0.1% NaN_3) and once with 50 mM TRIS pH 8.0, 100 mM NaCl. Washed inclusion bodies were denatured in 8 M urea, 50 mM MES pH 6.5, 1% DTT, 100 mM EDTA and denatured beta-2 microglobulin was injected dropwise into refolding buffer composed of 400 mM L-arginine, 100 mM TRIS pH 8.0, 2 mM EDTA, 5 mM reduced glutathione, 0.5 mM oxidized glutathione. After refolding for 1 hour at 4° C, VL9 peptide (Avantor) resuspended in DMSO was added to the refolding mixture to a final concentration of 20 μM. Denatured HLA-E heavy chain was then added to the refolding mixture in a dropwise manner and the complex was allowed to form

while stirring at 4° C for 48 hours. Refolded HLA-E-VL9 complex was then filtered through a 0.45 µm filter and purified by size-exclusion chromatography using a Superdex200 column (Cytiva) in 2 mM TRIS pH 8.0, 200 mM NaCl, 0.02% NaN_3.

Plasmids encoding the 3H4v31 heavy and light chains were transfected into FreeStyle293 cells using polyethylenimine. The 3H4v31 heavy chain was modified to include an HRV3C cleavage site between the Fab and Fc domains and a small truncation was made to the C_L domain to facilitate crystallization [61]. Protein was purified from filtered cell supernatants using ProteinA resin (Pierce) and purified IgG was digested into Fab using HRV3C protease.

3H4v31 Fab was mixed with a 1.5-fold molar excess of HLA-E-VL9 and binding was allowed to occur at 4° C for 1 hour. The complex was then purified by size-exclusion chromatography using a Superdex200 column in 2 mM TRIS pH 8.0, 200 mM NaCl, 0.02% NaN_3.

X-ray crystallography

The HLA-E-VL9 + 3H4v31 Fab complex was concentrated to 7.80 mg/mL and used to prepare several crystallization screens using an Oryx4 liquid handling device (Douglas Instruments). Crystals were obtained in a mother liquor composed of 20.1% PEG 1500, 2.01% MPD, 0.2 M magnesium sulfate, and 0.1 M sodium acetate pH 5.5. A single crystal was cryoprotected with mother liquor supplemented with 20% glycerol prior to plunge freezing in liquid nitrogen.

Diffraction data were collected at ALS Beamline 5.0.1. Data were indexed and integrated in iMOSFLM [62] before being merged and scaled in AIMLESS [63]. Despite purification of the intact complex, a molecular replacement solution could only be found for the 3H4v31 Fab, potentially due to the low pH of the mother liquor that facilitated crystallization. Molecular replacement was performed using PhaserMR **[64]**, with PDB ID: 7BH8 chains G and H as a search ensemble [46]. The 3H4v31 Fab molecular replacement solution was iteratively refined using Coot, Phenix and ISOLDE [65-67].

Chromium-51 (^{51}Cr) Release assay

Target cells were washed with complete media (RPMI 1640 with 10% FBS), resuspended at 1 x 10^7 cells per mL, and labeled with 250 μCi/mL of ^{51}Cr $Na_2{}^{51}CrO_4$. Cells were labeled for 1 hour and 20 minutes at 37°C then washed three times with R10. Labeled cells were mixed with test antibody at 2 μg/mL and effector cells in at least triplicate wells at the desired effector to target (E:T) ratios in 96-well round bottom plates. After 6 hours of co-culture , cells were pelleted by centrifugation. 25μL of supernatant was added to 150 μL of Ultima Gold LS Cocktail (Sigma) in a 96-well plate. Radioactivity was measured using the MicroBeta TriLux 1450 counter (Perkin Elmer). On every plate, ^{51}Cr labeled target cells without effector cells were included as a spontaneous release control, and 51Cr labeled target cells mixed with 2% Triton X-100 detergent were included as a maximum release control. The %^{51}Cr release of specific lysis was calculated for each well using the following formula: [(Experimental Release – Spontaneous Release)/(Maximum Release – Spontaneous Release)] × 100.

CD107a degranulation assay

Effector and target cells were washed with complete media (RPMI 1640 with 10% FBS) and co-cultured in 96-well plates, in the presence of BD GolgiPlug and BD GolgiStop protein transport inhibitors (BD Biosciences) at 1:1000 and 4:6000 concentration per manufacturer recommendation, and PE-conjugated anti-human CD107a antibody (clone H4A3, Biolegend) at 10 μg/mL. The effector:target cell ratio used was 2.5:1 for experiments using effectors NK-92 or NK-92. CD16, and at 5:1 for experiments using primary NK cells isolated from leukopheresis samples. After 6 hours of co-culture, cells were washed with PBS then stained with LIVE/DEAD Fixable Near-IR Dead Cell Stain Kit (ThermoFisher Scientific), followed by another wash with PBS and staining with fluorescently conjugated monoclonal antibodies against APC conjugated anti-human CD56 (clone 5.1H11, Biolegend) for 20 minutes at room temperature. Cells were washed with PBS then fixed in 2% PFA/PBS and run on a BD Fortessa or BD LSR II flow cytometer and analyzed using FlowJo software, version 10. Cells were gated on the basis of

size, viability, GFP, CD56, and CD107a expression. Percent of NK cells that were positive for CD107a was calculated as the percentage of live GFP-negative CD56-positive cells that were CD107a+.

Staining of human cell lines

SiHa or SU86.86 cell lines were released from cell culture plates by incubation with 5mM of EDTA in PBS for 3 minutes (SiHa) or 10 minutes (SU86.86) followed by two washes with PBS. Cells were then stained for viability with LIVE/DEAD Fixable Near-IR Dead Cell Stain (ThermoFisher Scientific) at 1:1000 at room temperature for 10 minutes. Following one wash in PBS, cells were stained with 3H4v31 IgG1 or isotype control CH65 at 4µg/mL at 4°C for 30 min followed by two washes with PBS, then stained with goat anti-human IgG cross-adsorbed secondary antibody in AF647 (ThermoFisher scientific) at 4°C for 30 min. Staining was performed in 100µL volume at 10 million cells per mL Following two washes with PBS, cells were fixed in 2% PFA/PBS and run on a BD Fortessa or BD LSR II flow cytometer and analyzed using FlowJo software, version 10.

Cell culture

K562 cells expressing a disulfide-trapped single-chain trimer of HLA-E-beta-2-microglobulin-VL9 (K562-HLA-E-VL9) were made from transduction of the MHC-I null lymphoblast cell line K562 with single chain trimer constructs encoding HLA-E*01:03 with the VL9 peptide VMAPRTLVL, as described in [48]. All other cell lines were obtained from the American Type Culture Collection (ATCC). K562 cells were cultured in RPMI-1640 media (ATCC) supplemented with 10% fetal bovine serum (Thermo Fisher Scientific) and 100 U/mL Penicillin-Streptomycin (Gibco). NK-92 cells were cultured in MyeloCult media (StemCell Technologies) supplemented with 1X Minimal Essential Media Non-essential amino acids solution (Gibco), 1 mM sodium pyruvate (Gibco), 1M HEPES (Gibco), 50 IU/mL penicillin/streptomycin (Gibco), and 100 IU/mL of HumanKine recombinant human interleukin 2 (Proteintech). NK-92.CD16 cells were obtained from the ATCC patent repository [49, 50] were also

cultured in MyeloCult media supplemented with 100 IU/mL of HumanKine recombinant human interleukin 2. SiHa cells were cultured in DMEM supplemented with 10% FBS. SU.86.86 were cultured in RPMI-1640 supplemented with 10% FBS. All cell lines were maintained at 37C and 5% CO2 in humidified incubators.

Isolation of primary human NK cells

Human leukapheresis frozen vials were collected by the External Quality Assurance Program Oversight Laboratory (EQAPOL). Samples were thawed and cultured overnight in RPMI-1640 supplemented with 10% FBS and 10 ng/mL of recombinant human IL-15 (abcam). NK cells were isolated using the EasySep Human NK Isolation Kit manufactured by StemCell Technologies.

Animals

NOD scid gamma (NSG) mice were purchased from The Jackson Laboratory. All animal experiments were conducted with approved protocols from the Duke University Institutional Animal Care and Use Committee.

Orthotopic K562 mouse model

NSG mice were subcutaneously implanted with K562-HLA-E-VL9 cells over the right flank. Treatments comprised of 10^6 PBS-washed NK-92 cells, 990 mcg of 3H4v31 or CH65 IgG, and 25000 IU of human IL-2, and delivered intratumorally on days indicated in the text. Tumors were measured daily using calipers. Mice were euthanized at a pre-defined tumor size endpoint (> 2000 mm3 for experiment in figure 3A , 3375 mm3 for experiments in figure 3B and 3C).

Immunohistochemistry

Tumors were excised in their entirety from the subcutaneous R flank. They were sectioned with a scalpel to fit into the OCT cassette, embedded in OCT compound (TFM media, General Data), and the

cassette placed on dry ice until the compound was frozen. Cassettes were stored at -80C. Sections (5 µm) were cut on a cryostat (Thermo Scientific CryoStar NX50) and placed on positively-charged glass slides Fisher Scientific) and stored at -80C. Prior to staining, slides were allowed to warm to RTP and then immediately fixed in 4% Formaldehyde (EMS) in fix buffer (10mM MES pH6.1, 125mM KCl, 3mM $MgCl_2$, 2mM EGTA, 10% Sucrose, all Sigma) for 10 mins. After washing in PBS, tissue was permeabilized with 0.2% Triton-X-100 (Invitrogen) in PBS for 5 mins and washed again with PBS. The samples were then incubated with Block-Aid (Thermo-Fisher) for 30 mins and then incubated with primary antibodies diluted in block for 1 hr. Primary antibodies- Goat anti-CD56 (1/400, AF2408, R&D), Rabbit anti-cleaved Caspase-3 (1/400, 9661, Cell Signaling technologies), Goat anti-CD16/32 (1/50, AF1460 R&D). Samples were washed 3x5 mins in PBS and then incubated with labelled secondary antibodies (Donkey anti-Goat Alexa 647, Donkey anti-Rabbit Rhodamine-Red-X, Donkey anti-Human Alexa 790, all Jackson-Immuno) for 45 minutes. Samples were then washed 6x10 mins in PBS, rinsed with water and mounted under #1.5 coverslips with Prolong Glass (Thermo-Fisher).

Image Acquisition

Slides were imaged using a Nikon 20X λD, 0.8 NA air objective on Nikon Eclipse Ti2 inverted microscope and using Elements acquisition software and LED illumination (Lumencor). Excitation filters: dichroic mirrors:emission filters used were – ET555/20x: T585lxpr: ET595/33m for Rhodamine-Red-X; ET635/30x: T660lpxr: ET697/60m for Alexa 647; FF01-735/28 (Semrock): T760lpxr: ET811/80m for Alexa 790- all filters and dichroics Chroma technology unless noted. Images were obtained using an Orca Fusion sCMOS camera (Hamamatsu). Whole tumor images were collected by stitching using Elements software and images were processed in Elements. Regions with high levels of NK-92 cells were selected for comparison of cleaved caspase staining while avoiding any areas that might contain frost damage.

Statistical Analysis

Data were plotted using Prism GraphPad version 9. For 51Cr release cytotoxic cell death assays and CD107a based degranulation assays, t-tests were applied to evaluate the indicated comparisons, and a P-value of < 0.05 was considered significant. P-values of < 0.05 are indicated with *, <0.01 with **, and <0.001 with ***. Kendall Tau correlations were used to test for a dose-dependent effect of antibody concentration on target cell killing. For in vivo mouse experiments, mixed effects models were used to compare tumor growth rates between treatment groups. No adjustments were made to the alpha level for multiple comparisons.

Acknowledgements:

We thank Duke Human Vaccine Institute (DHVI) programs and finance staff for project oversight and the contributions of technical staff at the DHVI, including Jordan Cocchiaro, Giovanna Hernandez, Esther Lee, Paige Power, Aja Sanzone, Brenna Harrington, Andrew Foulger, Amanda Newman, Pahvie Chhan, Cindy Bowman, Grace Stevens, Thad Gurley, Madison Berry, Kara Anasti, Katayoun Mansouri,Erika Dunford, and Dawn Jones Marshall. We thank the DHVI Flow Cytometry Core and Duke Cancer Institute Flow Cytometry Shared Resource (FCSR) for technical assistance. We thank Tom Denny for providing leukopheresis samples through EQAPOL (HHSN272201700061C). This study was funded by the Collaboratory of AIDS Researchers for Eradication (CARE; UM1AI164567) (B.F.H.) and the Bill and Melinda Gates Foundation OPP1108533 (A.J.M.). Support for this study was provided by the Duke Hematology & Transfusion Medicine Training Program (T32 HL007057) to J.K.H. P.B and A.J.M. are Jenner Institute Investigators.

References:

1. Tan, S., et al., *Immune Checkpoint Inhibitor Therapy in Oncology: Current Uses and Future Directions: JACC: CardioOncology State-of-the-Art Review.* JACC CardioOncol, 2022. **4**(5): p. 579-597.

2. Seidel, J.A., A. Otsuka, and K. Kabashima, *Anti-PD-1 and Anti-CTLA-4 Therapies in Cancer: Mechanisms of Action, Efficacy, and Limitations.* Front Oncol, 2018. **8**: p. 86.
3. Haslam, A. and V. Prasad, *Estimation of the Percentage of US Patients With Cancer Who Are Eligible for and Respond to Checkpoint Inhibitor Immunotherapy Drugs.* JAMA Netw Open, 2019. **2**(5): p. e192535.
4. Egen, J.G., W. Ouyang, and L.C. Wu, *Human Anti-tumor Immunity: Insights from Immunotherapy Clinical Trials.* Immunity, 2020. **52**(1): p. 36-54.
5. Jiang, Y., et al., *Progress and Challenges in Precise Treatment of Tumors With PD-1/PD-L1 Blockade.* Front Immunol, 2020. **11**: p. 339.
6. Trinchieri, G., *Biology of natural killer cells.* Adv Immunol, 1989. **47**: p. 187-376.
7. Kyrysyuk, O. and K.W. Wucherpfennig, *Designing Cancer Immunotherapies That Engage T Cells and NK Cells.* Annu Rev Immunol, 2023. **41**: p. 17-38.
8. Ljunggren, H.G. and K. Karre, *In search of the 'missing self': MHC molecules and NK cell recognition.* Immunol Today, 1990. **11**(7): p. 237-44.
9. Vyas, M., et al., *Natural killer cells suppress cancer metastasis by eliminating circulating cancer cells.* Front Immunol, 2022. **13**: p. 1098445.
10. Lopez-Soto, A., et al., *Control of Metastasis by NK Cells.* Cancer Cell, 2017. **32**(2): p. 135-154.
11. Liu, X., et al., *Immune checkpoint HLA-E:CD94-NKG2A mediates evasion of circulating tumor cells from NK cell surveillance.* Cancer Cell, 2023. **41**(2): p. 272-287 e9.
12. Shifrin, N., D.H. Raulet, and M. Ardolino, *NK cell self tolerance, responsiveness and missing self recognition.* Semin Immunol, 2014. **26**(2): p. 138-44.
13. Fantini, M., P.M. Arlen, and K.Y. Tsang, *Potentiation of natural killer cells to overcome cancer resistance to NK cell-based therapy and to enhance antibody-based immunotherapy.* Front Immunol, 2023. **14**: p. 1275904.
14. Andre, P., et al., *Differential regulation of killer cell Ig-like receptors and CD94 lectin-like dimers on NK and T lymphocytes from HIV-1-infected individuals.* Eur J Immunol, 1999. **29**(4): p. 1076-85.
15. Mahapatra, S., et al., *High-resolution phenotyping identifies NK cell subsets that distinguish healthy children from adults.* PLoS One, 2017. **12**(8): p. e0181134.
16. Braud, V., E.Y. Jones, and A. McMichael, *The human major histocompatibility complex class Ib molecule HLA-E binds signal sequence-derived peptides with primary anchor residues at positions 2 and 9.* Eur J Immunol, 1997. **27**(5): p. 1164-9.
17. Braud, V.M., et al., *HLA-E binds to natural killer cell receptors CD94/NKG2A, B and C.* Nature, 1998. **391**(6669): p. 795-9.
18. Lee, N., et al., *HLA-E surface expression depends on binding of TAP-dependent peptides derived from certain HLA class I signal sequences.* J Immunol, 1998. **160**(10): p. 4951-60.
19. Lee, N., et al., *HLA-E is a major ligand for the natural killer inhibitory receptor CD94/NKG2A.* Proc Natl Acad Sci U S A, 1998. **95**(9): p. 5199-204.
20. King, A., et al., *HLA-E is expressed on trophoblast and interacts with CD94/NKG2 receptors on decidual NK cells.* Eur J Immunol, 2000. **30**(6): p. 1623-31.
21. Borst, L., S.H. van der Burg, and T. van Hall, *The NKG2A-HLA-E Axis as a Novel Checkpoint in the Tumor Microenvironment.* Clin Cancer Res, 2020. **26**(21): p. 5549-5556.
22. Michaelsson, J., et al., *A signal peptide derived from hsp60 binds HLA-E and interferes with CD94/NKG2A recognition.* J Exp Med, 2002. **196**(11): p. 1403-14.
23. Wooden, S.L., et al., *Cutting edge: HLA-E binds a peptide derived from the ATP-binding cassette transporter multidrug resistance-associated protein 7 and inhibits NK cell-mediated lysis.* J Immunol, 2005. **175**(3): p. 1383-7.
24. Joosten, S.A., et al., *Mycobacterium tuberculosis peptides presented by HLA-E molecules are targets for human CD8 T-cells with cytotoxic as well as regulatory activity.* PLoS Pathog, 2010. **6**(2): p. e1000782.

25. McMurtrey, C., et al., *T cell recognition of Mycobacterium tuberculosis peptides presented by HLA-E derived from infected human cells.* PLoS One, 2017. **12**(11): p. e0188288.
26. Hansen, S.G., et al., *Broadly targeted CD8(+) T cell responses restricted by major histocompatibility complex E.* Science, 2016. **351**(6274): p. 714-20.
27. Mbiribindi, B., et al., *Epstein-Barr virus peptides derived from latent cycle proteins alter NKG2A + NK cell effector function.* Sci Rep, 2020. **10**(1): p. 19973.
28. Vietzen, H., et al., *HLA-E-restricted immune responses are crucial for the control of EBV infections and the prevention of PTLD.* Blood, 2023. **141**(13): p. 1560-1573.
29. Gooden, M., et al., *HLA-E expression by gynecological cancers restrains tumor-infiltrating CD8(+) T lymphocytes.* Proc Natl Acad Sci U S A, 2011. **108**(26): p. 10656-61.
30. Bianchini, M., et al., *Comparative study of gene expression by cDNA microarray in human colorectal cancer tissues and normal mucosa.* Int J Oncol, 2006. **29**(1): p. 83-94.
31. Zhen, Z.J., et al., *Impact of HLA-E gene polymorphism on HLA-E expression in tumor cells and prognosis in patients with stage III colorectal cancer.* Med Oncol, 2013. **30**(1): p. 482.
32. Levy, E.M., et al., *Human leukocyte antigen-E protein is overexpressed in primary human colorectal cancer.* Int J Oncol, 2008. **32**(3): p. 633-41.
33. Talebian Yazdi, M., et al., *The positive prognostic effect of stromal CD8+ tumor-infiltrating T cells is restrained by the expression of HLA-E in non-small cell lung carcinoma.* Oncotarget, 2016. **7**(3): p. 3477-88.
34. McWilliams, E.M., et al., *Therapeutic CD94/NKG2A blockade improves natural killer cell dysfunction in chronic lymphocytic leukemia.* Oncoimmunology, 2016. **5**(10): p. e1226720.
35. Barrett, D.M., et al., *A GATA factor mediates cell type-restricted induction of HLA-E gene transcription by gamma interferon.* Mol Cell Biol, 2004. **24**(14): p. 6194-204.
36. Nguyen, S., et al., *HLA-E upregulation on IFN-gamma-activated AML blasts impairs CD94/NKG2A-dependent NK cytolysis after haplo-mismatched hematopoietic SCT.* Bone Marrow Transplant, 2009. **43**(9): p. 693-9.
37. Fisher, J.G., et al., *XPO1 inhibition sensitises CLL cells to NK cell mediated cytotoxicity and overcomes HLA-E expression.* Leukemia, 2023. **37**(10): p. 2036-2049.
38. Hiraoka, N., et al., *Expression of classical human leukocyte antigen class I antigens, HLA-E and HLA-G, is adversely prognostic in pancreatic cancer patients.* Cancer Sci, 2020. **111**(8): p. 3057-3070.
39. Sun, C., et al., *High NKG2A expression contributes to NK cell exhaustion and predicts a poor prognosis of patients with liver cancer.* Oncoimmunology, 2017. **6**(1): p. e1264562.
40. Stringaris, K., et al., *Leukemia-induced phenotypic and functional defects in natural killer cells predict failure to achieve remission in acute myeloid leukemia.* Haematologica, 2014. **99**(5): p. 836-47.
41. Bossard, C., et al., *HLA-E/beta2 microglobulin overexpression in colorectal cancer is associated with recruitment of inhibitory immune cells and tumor progression.* Int J Cancer, 2012. **131**(4): p. 855-63.
42. Andre, P., et al., *Anti-NKG2A mAb Is a Checkpoint Inhibitor that Promotes Anti-tumor Immunity by Unleashing Both T and NK Cells.* Cell, 2018. **175**(7): p. 1731-1743 e13.
43. J. Fayette, L.F.L.L., K. J. Harrington, R. Hadded, L. L. Siu, Y. C. Liu, M. Tahara, J-P Machiels, D. Rischin, T. Sweiwert, R. Ferris, U. Keilholz, A. Psyrri, B. Keam, P. Bossi, R. Metcalf, O. Serrano, P. Kaur, D. Ruscica, R. B. Cohen, *Phase III study of cetuximab (CTX) ± monalizumab (M) in participants (pts) with recurrent/metastatic head and neck squamous cell carcinoma (R/M HNSCC) with disease progression on/after platinum chemotherapy (CT) and previously treated with an immune checkpoint inhibitor (ICI)*, in *European Society for Medical Oncology* . 2023.
44. Clynes, R.A., et al., *Inhibitory Fc receptors modulate in vivo cytotoxicity against tumor targets.* Nat Med, 2000. **6**(4): p. 443-6.

45. Li, F. and S. Liu, *Focusing on NK cells and ADCC: A promising immunotherapy approach in targeted therapy for HER2-positive breast cancer.* Front Immunol, 2022. **13**: p. 1083462.
46. Li, D., et al., *Mouse and human antibodies bind HLA-E-leader peptide complexes and enhance NK cell cytotoxicity.* Commun Biol, 2022. **5**(1): p. 271.
47. Whiteside, T.L., *Measurement of cytotoxic activity of NK/LAK cells.* Curr Protoc Immunol, 2001. **Chapter 7**: p. Unit 7 18.
48. Yang, H., et al., *HLA-E-restricted, Gag-specific CD8(+) T cells can suppress HIV-1 infection, offering vaccine opportunities.* Sci Immunol, 2021. **6**(57).
49. Binyamin, L., et al., *Blocking NK cell inhibitory self-recognition promotes antibody-dependent cellular cytotoxicity in a model of anti-lymphoma therapy.* J Immunol, 2008. **180**(9): p. 6392-401.
50. Pazina, T., et al., *Enhanced SLAMF7 Homotypic Interactions by Elotuzumab Improves NK Cell Killing of Multiple Myeloma.* Cancer Immunol Res, 2019. **7**(10): p. 1633-1646.
51. Lo, M., et al., *Effector-attenuating Substitutions That Maintain Antibody Stability and Reduce Toxicity in Mice.* J Biol Chem, 2017. **292**(9): p. 3900-3908.
52. Yeap, W.H., et al., *Corrigendum: CD16 is indispensable for antibody-dependent cellular cytotoxicity by human monocytes.* Sci Rep, 2017. **7**: p. 46202.
53. Laboratory, T.J. *Frequently Asked NSG(TM) Questions*. 2024 7/1/24]; Available from: https://www.jax.org/jax-mice-and-services/find-and-order-jax-mice/nsg-portfolio/frequently-asked-nsg-questions.
54. Saunders, K.O., *Conceptual Approaches to Modulating Antibody Effector Functions and Circulation Half-Life.* Front Immunol, 2019. **10**: p. 1296.
55. Fabian, K.P. and J.W. Hodge, *The emerging role of off-the-shelf engineered natural killer cells in targeted cancer immunotherapy.* Mol Ther Oncolytics, 2021. **23**: p. 266-276.
56. Laskowski, T.J., A. Biederstadt, and K. Rezvani, *Natural killer cells in antitumour adoptive cell immunotherapy.* Nat Rev Cancer, 2022. **22**(10): p. 557-575.
57. Keener, A.B., *Natural killer cells show their cancer-fighting worth.* Nature, 2024. **629**(8014): p. S4-S6.
58. Kaiser, B.K., et al., *Structural basis for NKG2A/CD94 recognition of HLA-E.* Proc Natl Acad Sci U S A, 2008. **105**(18): p. 6696-701.
59. Fisher, J.G., et al., *Selinexor Enhances NK Cell Activation Against Malignant B Cells via Downregulation of HLA-E.* Front Oncol, 2021. **11**: p. 785635.
60. Vietzen, H., et al., *Ineffective control of Epstein-Barr-virus-induced autoimmunity increases the risk for multiple sclerosis.* Cell, 2023. **186**(26): p. 5705-5718 e13.
61. Lieu, R., et al., *Rapid and robust antibody Fab fragment crystallization utilizing edge-to-edge beta-sheet packing.* PLoS One, 2020. **15**(9): p. e0232311.
62. Battye, T.G., et al., *iMOSFLM: a new graphical interface for diffraction-image processing with MOSFLM.* Acta Crystallogr D Biol Crystallogr, 2011. **67**(Pt 4): p. 271-81.
63. Evans, P.R. and G.N. Murshudov, *How good are my data and what is the resolution?* Acta Crystallogr D Biol Crystallogr, 2013. **69**(Pt 7): p. 1204-14.
64. McCoy, A.J., *Solving structures of protein complexes by molecular replacement with Phaser.* Acta Crystallogr D Biol Crystallogr, 2007. **63**(Pt 1): p. 32-41.
65. Emsley, P. and K. Cowtan, *Coot: model-building tools for molecular graphics.* Acta Crystallogr D Biol Crystallogr, 2004. **60**(Pt 12 Pt 1): p. 2126-32.
66. Adams, P.D., et al., *PHENIX: a comprehensive Python-based system for macromolecular structure solution.* Acta Crystallogr D Biol Crystallogr, 2010. **66**(Pt 2): p. 213-21.
67. Croll, T.I., *ISOLDE: a physically realistic environment for model building into low-resolution electron-density maps.* Acta Crystallogr D Struct Biol, 2018. **74**(Pt 6): p. 519-530.